

Structural Design Optimization and Construction Technology Research on Rigid-Frame Bridge Wind Resistance Enhancement

Jian'an Zheng¹, Fengwu Yu², Jun Tang^{2,*} and Chuanyang Yang²

¹ Guangxi Pinglu Canal Construction Co., Ltd., Nanning, Guangxi, 530023, China

² CCCC First Highway Engineering Group Co., Ltd., Beijing, 100000, China

Corresponding authors: (e-mail: lunwenei333@163.com).

Abstract According to the principle of operability of Rigid-Frame Bridge project, the structural design optimization plan for wind resistance of Rigid-Frame Bridge is proposed, which mainly focuses on the design optimization of bridge superstructure and substructure. Combined with the current mainstream Rigid-Frame Bridge construction technology, the overall construction plan and box girder construction plan are formulated, and the construction optimization plan is put forward to avoid the problem of time lag. With the help of finite element model, the structural design optimization and construction technology of Rigid-Frame Bridge are simulated and analyzed. The maximum lateral displacement of 12.9cm occurs at the maximum cantilever stage of the pier top, and the cross-section stress at the bottom of the pier is 1.762MPa tensile stress, which does not exceed the permissible value. The error between the measured line (stress value) and the theoretical line (stress value) of the girder section from 1# to 9# during the cantilever stage of the construction is within the permissible value of the project, which verifies that the simulation model is reliable and lays a foundation of the subsequent research.

Index Terms rigid frame bridge, wind resistance, structural design optimization, construction technology, finite element model

I. Introduction

As an important part of modern transportation systems, steel bridges bear the role of vehicle loads and natural environmental forces. Under severe climatic conditions, such as strong winds and earthquakes and other natural disasters, the wind resistance and vibration control of bridge structures are particularly important [1]-[4]. Steel bridges are affected by wind loads under the action of wind, which are mainly manifested by the vibration of the bridge and the action of side wind forces. These wind loads pose a threat to the stability and safety of bridge structures, so controlling wind loads is crucial for bridge design and construction [5]-[8].

Wind vibration phenomenon is the vibration phenomenon that occurs in bridges under the action of wind. When the airflow passes through the bridge structure, it will cause the change of aerodynamic coefficient, which leads to the vibration of the bridge structure. This vibration will not only affect the service life of the bridge, but also bring threats to the safety of traveling [9]-[12]. Under strong wind conditions, the bridge structure will have a lateral effect on the bridge structure, causing the bridge to be deflected. If not controlled, the lateral wind force may lead to the collapse of the bridge. Therefore, wind-resistant measures are essential in bridge design and construction [13]-[16]. In order to ensure the safety and stability of bridge structures, wind and vibration control is required for steel bridges. Commonly used control methods include, bridge structural design, wind tunnel test, damping control and construction technology, etc. All these control methods can strengthen the wind resistance performance of Rigid-Frame Bridges to a certain extent, so as to enhance the life and safety of the bridge [17]-[20].

Taking a bridge as the engineering background, the structural design and construction technology of wind resistance of Rigid-Frame Bridge are studied. Under the requirements of technical standards, the upper and lower parts of Rigid-Frame Bridge are designed, and the principle of calculating the static (dynamic) wind load of the bridge and differential equations are established by investigating the mutual force between wind and the bridge structure. Utilizing the most advanced construction technology, the overall construction plan and box girder construction plan are planned. Integrating the structural design of the wind-resistant Rigid-Frame Bridge, planning the overall construction plan and box girder construction plan, and establishing the finite element simulation model of Rigid-Frame Bridge using Midas Civil. Compare the measured results of bridge parameters with the simulation results to confirm the reasonableness of the finite element model, in order to successfully complete the structural design optimization work.

II. Structural design and construction techniques for wind resistance of Rigid-Frame Bridges

II. A. Overview of Rigid-Frame Bridges and Project Profile

II. A. 1) Overview of Rigid-Frame Bridges

As a main bridge type of prestressed concrete bridge, although this bridge type has the competitive advantages of large span, reasonable force, convenient construction, etc., it is greatly affected by the shrinkage creep of concrete, which often leads to the deflection of the middle span, the web and the cracking of the bottom plate, and therefore increases the difficulty of the bridge's later maintenance [21], [22]. Combining the structural advantages of continuous steel bridges and the effect of concrete shrinkage creep, it is found that the steel girder combined rigid structure-continuous combined girder bridge is the best solution.

II. A. 2) Summary of works

A bridge according to its own bridge status quo, developed a 120m + 4250m + 120m continuous rigid span configuration program. The main pier location is used in the form of pier-beam consolidation, the consolidation section is relatively long, and the side pier stress condition is worrisome. Therefore, in the case of considering the use of large-tonnage bearings at the side piers, a mixed system of continuous beams and continuous stiffeners is adopted. In order to effectively reduce the main span after the bridge due to concrete shrinkage, creep caused by the main pier has a large bending moment as well as the phenomenon of mid-span deflection, in the main pier periphery and the side spans are still used in the position of the concrete beams, the position of the mid-span use of steel box girders, by this way to reduce the main span of the deadweight, reduce the deflection of the late stage, and at the same time can prevent the main pier due to the temperature force, the concrete shrinkage and creep produced by the tensile stresses, and effectively improve the main pier and main girder bearing capacity, the main pier and main girder bearing capacity. The main pier as well as the main girder stress condition, so that the burden of the lower foundation is greatly reduced, but also able to reduce the beam height.

II. B. Structural Design Optimization for Wind Performance of Rigid Bridges

II. B. 1) Main technical standards

- (1) Highway grade: Grade II.
- (2) Design speed: 80km/h.
- (3) Design base period: 140 years.
- (4) Design service life: 140 years for special bridge and bridge.
- (5) Environmental category: Class I.
- (6) Design safety level of bridge: Class I.
- (7) Design load level: Highway Class I.
- (8) Design Flood Frequency: 1/500 for special bridge, big bridge and middle bridge, normal storage level of a hydropower station is 812m, and dead water level is 758m.
- (9) Slope of bridge deck: 4% of two-way cross slope of bridge deck.
- (10) Bridge width: standard width of the bridge deck 0.4m guardrail + 8.8m carriageway + 0.3m guardrail = 9.5m.
- (11) The level of bridge seismic defense measures: large, large bridge according to 9 degrees of defense.
- (12) Navigational requirements: there is no navigational requirement in the scope of this route.
- (13) Coordinate system, elevation benchmark: 2008 a city coordinate system, 2013 national elevation benchmark.

II. B. 2) Superstructure

The cross-section of the main girder is shown in Figure 1. The main bridge superstructure adopts 120m+4250m+120m variable section prestressed concrete continuous rigid structure, the box girder adopts single box and single chamber section, the top width is 9.5m, the bottom width is 4.8m, the length of cantilever is 2.12m, the thickness of the cantilever end is 0.33m, and the thickness of the root is 0.62m, the top plate is connected to the web with the bearing bracket of 1.44×0.39m, and the bottom plate is connected to the web with all the 0.42 × 0.27m chamfer. The root girder height is 6.72m, the end girder height is 2.71m, and the center girder height varies according to the quadratic parabolic form. The thickness of the web at the root is 0.61m, the thickness of the web at the middle of the span is 0.41m, and it varies linearly in the vicinity of L/4 through two sections. The top slab is 0.28m thick and the bottom slab thickness varies from 0.28m at the end by quadratic parabola to 0.78m at the root. Block 0 has a top slab of 0.42m thick, a bottom slab of 1.2m thick and a web of 1.2m thick. The box girder is provided with crossbeam at each pivot point, the end crossbeam is 1.5m thick, the middle crossbeam is 2 × 1m thick, and the middle span is provided with a cross partition plate, the thickness of cross partition plate is 0.2m.

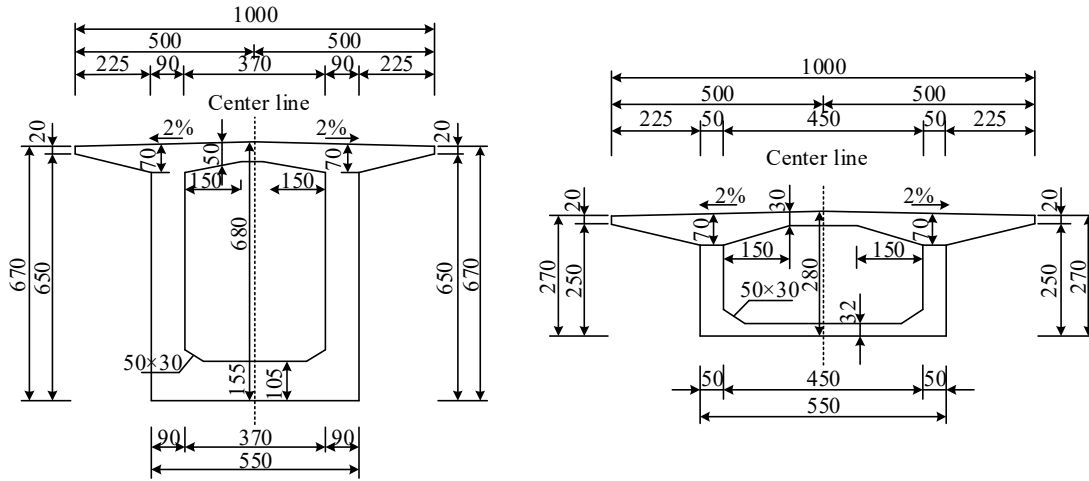


Figure 1: Cross section of the main beam

Rigid-frame box girder and cast-in-place monolithic bridge deck (including wet joints and concrete leveling layer) are made of C50 concrete, and the box girder adopts longitudinal, transverse and vertical three-way prestressing system. The longitudinal and transverse prestressing steel reinforcement adopts $f_{pk}=1860\text{MPa}$, $E_s=1.86\times 10^5\text{MPa}$ Φ^s 14.6mm steel strand (Class II relaxation), plastic bellows into holes, and vacuum-assisted grouting process. JL32 fine-rolled rebar with $f_{pk}=925\text{MPa}$ was used as the vertical prestressing reinforcement, pre-embedded metal bellows to form holes, and conventional prestressing hole grouting process.

II. B. 3) Substructure

Bridge substructure No.0 platform adopts pile-joined cover girder type abutment, with foundation of 2 Φ 1.3m piles.No.10 platform adopts U-shaped solid platform, with foundation of 6 Φ 1.3m piles. The main pier adopts box-shaped hollow pier, with cross-section size of 5.2 \times 5.3m in transverse direction \times shun bridge direction, wall thickness of 0.4m, bearing platform thickness of 4.2m, foundation of 8 Φ 1.5m piles. The transition pier adopts thin-walled solid pier, with cross-section dimension of 5.5 \times 2.1m in transverse direction \times 2.1m in downward direction, bearing thickness of 2m, foundation of 6 Φ 1m grouted pile foundation. Approach bridge pier 1~3 adopts double-column pier, column diameter Φ 1.4m, foundation for 2 Φ 1.3m grouted pile foundation. 8, 9 pier adopts double-column pier, column diameter Φ 1.2m, foundation for 2 Φ 1.7m grouted pile foundation. The main pier hollow pier body is made of C40 concrete, steel is made of Q235 steel, and the exposed surfaces are galvanized to prevent corrosion.

II. B. 4) Wind effects on bridge structures

(1) Climatic conditions

When the wind season comes, the wind load on the bridge structure has a greater impact, especially in the high pier large-span continuous Rigid-Frame Bridge maximum cantilever construction stage, when the bridge stability is poor, under the action of wind load is easy to instability damage. The fundamental reason for the bridge wind load is that when the wind flows through the bridge, the original flow field of the wind has changed. In the process of bridge wind load research, the role of the wind on the bridge is usually divided into static action and dynamic action.

(2) The static action of the wind and the three-part force

(a) Static effect of wind

The hydrostatic effect of wind means that the average wind of nature acts on the structure and produces a kind of static pressure effect on the structure. On the other hand, when the wind flows through the bridge structure, assuming that the bridge does not move, i.e., the bridge can be regarded as a fixed rigid body, at this time the static pressure effect can be equated to the role of uniform load.

When the wind flows through the structure, the wind flow line satisfies Bernoulli's equation:

$$\frac{1}{2}\rho U^2 + P = \text{Constant} \quad (1)$$

where U - wind speed, ρ - Air density, P - pressure.

According to formula (1), wind speed is proportional to air density and inversely proportional to pressure. In other conditions do not become the case, when the wind speed is greater, the pressure around the bridge section is less at this time. On the other hand, when the wind speed is larger, the incoming wind air density is smaller at this time.

(b) Static three-part force of wind

The lift force on the bridge is an integral of the difference in pressure between the upper and lower surfaces of the bridge section. The drag force is the integral of the pressure difference between the front and rear surfaces of the bridge: the torque is generated by the difference between the point of action of the combined lift and drag loads and the location of the center of gravity of the bridge section. Therefore, lift F_V , drag F_H , and torque M are the three main forces generated by wind loads. The three-force action of wind load in the body-axis coordinate system is shown in Fig. 2.

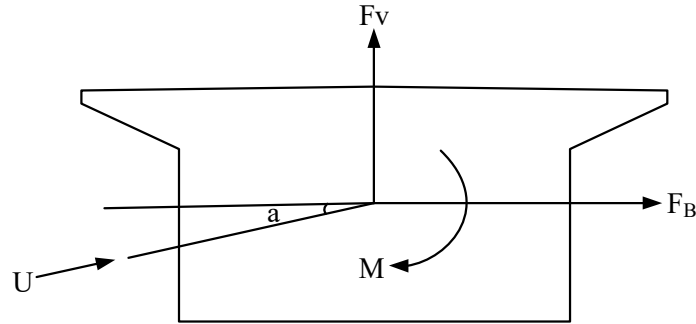


Figure 2: The wind load is three component force in the body axis coordinate system

According to the conditions under which wind loads arise is due to the fact that the wind flow through the bridge section changes the distribution and characteristics of the flow field. Other things being equal, the wind loads on two sections of similar shape are proportional to their characteristic dimensions, and the static wind loads on the bridge in the body-axis coordinate system are expressed in terms of dimensionless static three-part force coefficients:

$$F_H = \frac{1}{2} \rho U^2 C_H D \quad (2)$$

$$F_V = \frac{1}{2} \rho^2 C_V B \quad (3)$$

$$M = \frac{1}{2} \rho U^2 C_M B^2 \quad (4)$$

where ρ is the air density, D and B are the height and width of the bridge section, respectively, C_H , C_V and C_M are the drag coefficient, lift coefficient and torque coefficient in the body axis coordinate system, respectively:

(3) Dynamic effect of wind

The characteristics of the wind, the dynamic characteristics of the bridge structure, the interaction between the wind and the bridge structure of these three aspects affect the dynamic effect of the wind on the bridge. If the bridge structure stiffness is relatively large, the bridge does not vibrate under the action of the wind load, the bridge structure remains stationary, at this time the role of the wind on the bridge can be viewed as a static effect. If the bridge structure stiffness is small, the bridge structure vibration, the bridge structure wind load response generally has dynamic and static response. Under the action of wind load, the bridge structure produces vibration, and at the same time the bridge structure reacts to the flow field around the bridge. In general, the bridge in the near-ground wind under the action of its dynamic response is divided into two categories, one for the average wind action of the bridge structure from the flowing wind to absorb the energy generated by the self-excited vibration. The four manifestations of institutional vibration are: vortex vibration, shaking vibration, galloping vibration, and chattering vibration, of which chattering vibration and galloping vibration are scattered self-excited vibration. Another category is the pulsating wind action of the bridge structure produced by the forced vibration, generally manifested as the bridge structure accompanied by the vibration phenomenon.

(4) Effect of wind on bridge structure

According to "Highway Bridge Wind Resistance Design Code" JTG/T 3360-01-2018, the wind effect on bridge structure is generally divided into static effect, static wind effect and dynamic effect.

(5) Fluid mechanics control equation

Fluid flow obeys the physical conservation laws, namely: the law of conservation of mass, the law of conservation of energy and the law of conservation of momentum. A brief description of these three conservation laws is given below in terms of the governing equations [23].

(a) Mass conservation equation

Any fluid satisfies the law of conservation of mass, i.e., for an incompressible fluid, the mass of the fluid is equal for inflow and outflow into an enclosed space. According to the law of conservation of mass the equation of conservation of mass of a fluid, i.e., the equation of continuity, can be derived. That is:

$$\frac{\partial \rho}{\partial t} + \frac{\partial \rho \mu_x}{\partial x} + \frac{\partial \rho \mu_y}{\partial y} + \frac{\partial \rho \mu_z}{\partial z} = 0 \quad (5)$$

Introducing the vector symbol $div a = \frac{\partial a_x}{\partial x} + \frac{\partial a_y}{\partial y} + \frac{\partial a_z}{\partial z}$, Eq. (5) follows:

$$\frac{\partial \rho}{\partial t} + div(\rho \mu) = 0 \quad (6)$$

The symbol ∇ is introduced to denote the scatter, $\nabla \cdot a = div a = \frac{\partial a_x}{\partial x} + \frac{\partial a_y}{\partial y} + \frac{\partial a_z}{\partial z}$, so Eq. (6) can also be written as:

$$\frac{\partial \rho}{\partial t} + \nabla \cdot (\rho \mu) = 0 \quad (7)$$

In Eqs. (5) to (7), ρ is the density, t is the time, and μ is the velocity vector.

The above is the continuity equation for a transient three-dimensional compressible fluid. If the fluid is incompressible and the density ρ is constant, Eq. (5) can be changed to:

$$\frac{\partial u}{\partial x} + \frac{\partial v}{\partial y} + \frac{\partial w}{\partial z} = 0 \quad (8)$$

If the fluid flow is in steady state, the density ρ does not change with time and equation (8) can be changed to:

$$\frac{\partial \rho u}{\partial x} + \frac{\partial \rho v}{\partial y} + \frac{\partial \rho w}{\partial z} = 0 \quad (9)$$

(b) Equation of conservation of momentum

Like the law of conservation of mass, any fluid follows the law of conservation of momentum, which is in essence Newton's second law. According to the law of conservation of momentum, the equation of conservation of momentum in the direction of x , y and z axes can be written as:

$$\frac{\partial \rho u}{\partial t} + div(\rho u \mu) = -\frac{\partial p}{\partial x} + \frac{\partial \tau_{xx}}{\partial x} + \frac{\partial \tau_{yx}}{\partial y} + \frac{\partial \tau_{zx}}{\partial z} + F_x \quad (10)$$

$$\frac{\partial \rho v}{\partial t} + div(\rho v \mu) = -\frac{\partial p}{\partial y} + \frac{\partial \tau_{xy}}{\partial x} + \frac{\partial \tau_{yy}}{\partial y} + \frac{\partial \tau_{zy}}{\partial z} + F_y \quad (11)$$

$$\frac{\partial \rho w}{\partial t} + div(\rho w \mu) = -\frac{\partial p}{\partial z} + \frac{\partial \tau_{xz}}{\partial x} + \frac{\partial \tau_{yz}}{\partial y} + \frac{\partial \tau_{zz}}{\partial z} + F_z \quad (12)$$

where, p is the pressure exerted on the fluid microelement. τ_{xx} , τ_{yy} and τ_{zz} are the components of the viscous stress τ acting on the microelement by molecular viscosity, respectively. F_x , F_y and F_z are the volume forces on the microelement.

(c) Energy conservation equation

The law of conservation of energy is the law followed in the state of fluid with heat exchange, which is in essence the first law of thermodynamics. The energy conservation equation can be derived from the law of conservation of energy. That is:

$$\frac{\partial(\rho T)}{\partial t} + div(\rho \mu T) = div \left[\frac{k}{c_p} \cdot grad T \right] + S_T \quad (13)$$

Write it as an expansion:

$$\begin{aligned} & \frac{\partial(\rho T)}{\partial t} + \frac{\partial(\rho u T)}{\partial t} + \frac{\partial(\rho v T)}{\partial t} + \frac{\partial(\rho w T)}{\partial t} \\ & = \frac{\partial}{\partial x} \left(\frac{k}{c_p} \frac{\partial T}{\partial x} \right) + \frac{\partial}{\partial y} \left(\frac{k}{c_p} \frac{\partial T}{\partial y} \right) + \frac{\partial}{\partial z} \left(\frac{k}{c_p} \frac{\partial T}{\partial z} \right) + S_T \end{aligned} \quad (14)$$

where c_p is the specific heat capacity, T is the thermodynamic temperature, k is the heat transfer coefficient of the fluid, S_T is the internal heat source of the fluid and the portion of the fluid's mechanical energy that is converted to thermal energy under the effect of viscosity, also referred to as S_T is the viscous dissipation term.

II. C. Construction Technology Program

II. C. 1) General construction program

In the construction process, the most unfavorable cross-section position of the main girder is selected as the 1/4 position of the side span and the middle span, the pivot point of the girder span, and the mid-span position, and the most unfavorable cross-section position of the main pier is selected as the 10m position of the pier bottom. The main pier is constructed by climbing mold, and the girder pier top 0 girder section and side span 14 girder end are constructed by cast-in-place concrete with bracket, and the girder section from 1 to 9 is constructed by hanging concrete with triangular hanging basket.

II. C. 2) Box girder construction program

(1) After completing the overall construction of the piers, casting of block 0 was carried out on the brackets.

(2) Adopt balanced cantilever method to cast box girder, the casting order is symmetrical from the top of the pier to the middle of the span, in the construction to the 12th and 12' beam section, the bracket pre-pressure at the same time for the side-span cast-in-place section of the bracket, and then the side-span cast-in-place section is cast in place. After the casting was completed and the age and strength of the concrete met the design requirements, the transverse prestressing steel beams, longitudinal prestressing steel beams in the top plate (bottom plate), vertical prestressing steel reinforcement, and the bending steel beams under the web plate were tensioned accordingly.

(3) Removal of cantilever construction hanging baskets, at this time the bridge structure forms the largest single "T" state, cantilever casting girder section construction is completed.

(4) Carry out the installation of side-span closing section hangers (at the same time hangers pre-pressure) and counterweights, at the same time, the positioning of the rigid skeleton installation and locking, the entire installation process and locking of the ambient temperature needs to be strictly controlled at $10\text{ }^{\circ}\text{C} \sim 15\text{ }^{\circ}\text{C}$.

(5) The construction steps of the middle span closing section are similar to those of the side span closing section (4), and will not be repeated.

(6) The whole bridge is closed and the construction of the bridge deck system is completed.

II. C. 3) Construction Optimization Program

(1) Combined with the construction process causes schedule lag, put forward the construction optimization plan.

No.5 pier column section construction using climbing system support, and bear the self-weight, construction load, a section after the completion of pouring to drive the whole system automatically climb to the next section to be poured, until the completion of the pier construction.

(a) According to the height of the pier to determine the height, type and number of standard sections of the tower crane, the use of C7022 type tower crane. Construction of tower crane standard section due to insufficient number of problems not installed in a timely manner, so the site needs more spare tower crane standard section, the construction process combined with the site conditions, the best one-time installation of the tower crane in place.

(b) climbing mold template early into the field and assembly, climbing mold device installation process climbing mold assembly parts missing caused by climbing mold template assembly is not in place, the need for embedded parts, brackets, load-bearing tripod, back device, attached to the wall load-bearing devices, guide rails, hydraulic cylinders, hydraulic pumping station console, hydraulic valves, synchronous valves, power distribution devices, hoses, materials for inventory.

(2) In the construction process of Block 0, combined with the construction site schedule lag and other conditions, put forward the optimization plan for Block 0 and hanging basket construction.

(a) Not in time to organize the processing of brackets caused by the schedule lag, need to be in the pier before the top of the brackets need to be processed, and then use the abutment climbing formwork construction platform to install the brackets, climbing formwork construction platform demolition and the installation of block 0 templates synchronized.

(b) Bracket installation is completed after the pre-pressure, the need for pre-embedded angle converted to tension stress to determine the type of jack and the number of prestressing steel strand, and at the end of the installation of anchorage to prevent wire slip. In order to prevent deformation during tensioning platform production, the means to increase the stiffness is taken, and a 5cm thick steel plate is added in front of the anchorage.

(c) After completing the tensioning of block 0, it is necessary to dismantle the outer template and bracket in time, and assemble the main truss of hanging basket in advance, which can be lifted directly when used, and greatly shorten the installation time of the hanging basket. After completing the tensioning of block 1, the walking of the hanging basket is carried out, and the measuring group needs to release the samples in advance, and the template elevation is adjusted.

(d) Reinforcing steel, bellows in advance of the transfer to the construction site and regular inventory. According to the height of the pier to determine the concrete pump truck model and the number of delivery pipe, pier 5, 6 car pump pumping outlet pressure of 23MPa, the construction process combined with the site construction machinery is best to be fixed until the completion of the section block construction.

III. Optimization of structural design and analysis of construction techniques

III. A. Finite element modeling

According to the structural design of the wind-resistant performance of Rigid-Frame Bridge, planning the overall construction program and the box girder construction program, Midas Civil was used to establish a finite element simulation model of the whole bridge, so as to obtain the deformation and internal force of the main girder at each construction stage, and a total of 173 nodes and 156 units were built in the model of the whole bridge. The type and number of units used in each member of the model and the number of units divided by the member are shown in Table 1. Based on the data in the table, it can be seen that the number of units divided into 104 for the main girders and 55 for the main piers. The structural design optimization and construction technology of Rigid-Frame Bridge are simulated and analyzed with the help of the finite element model, and the specific analysis process and results will be given in the following.

Table 1: List of all units for each component

No.	Category	Adoption unit	Quantity	Divide the units.
1	Kingbeam	Beam unit	1	104
2	Main pier	Beam unit	2	55

III. B. Structural design optimization analysis

III. B. 1) Description of the experiment

Using balanced cantilever construction of continuous Rigid-Frame Bridge super-high pier wind safety is mainly reflected in the maximum cantilever construction stage response, for Rigid-Frame Bridge wind-resistant structural design optimization process of a total of five T-structure, in the simulation analysis using static wind load and the dynamic wind load of the structure of the comparative analysis of the box girder and abutment unit coordinate system as shown in Fig. 3, the comprehensive consideration of the role of the steel reinforcement, the strong skeleton and the role of the concrete. At the same time, in order to focus on testing the effectiveness of the wind-resistant construction measures of the super-high pier, the left and right widths of the two single T coupling consideration, the establishment of the super-high pier refined numerical model. Static wind load calculation, the main pier single T maximum cantilever stage of the static wind load, as a static load applied directly to the finite element model.

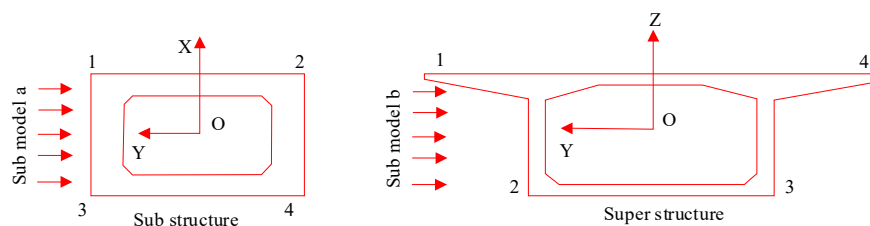


Figure 3: box beam and bridge block

Table 2: Lateral displacement of bridge structure caused by wind load

Analysis case	Static wind loading model				Dynamic wind loading model (sub-model a, sub-model b)			
	Largest d for box girder/cm		Largest d for pier/cm		Largest d for box girder/cm		Largest d for pier/cm	
	Location	Y direction	Location	Y direction	Location	Y direction	Location	Y direction
Without straining beam of wind bracing	Max cantilever section	7.6	Pier top section	6.8	Max cantilever section	25.7	Pier top section	26.5
with straining beam of wind bracing		4.2		2.7		12.9		10.6

III. B. 2) Lateral Displacements and Stresses in Bridge Structures

The lateral displacement results of the bridge structure 9# super-high pier pier caused by wind load are shown in Table 2. Only the action of dynamic wind load caused by the 9 # pier key cross-section stress results shown in Table 3, in order to reflect the tensile side stress, the pier bottom cross-section stress for the stress results of the 1' point in Figure 3, the construction stage of the box girder cross-section stress for the stress results of the 1 point (box girder top plate).

Table 3: Structural stress caused by wind load

Analysis case	Static wind loading model		Dynamic wind loading model (sub-model a, sub-model b)	
	Location	Stress/Mpa	Location	Stress/Mpa
Without straining beam of wind bracing	Bottom of pier	-0.883	Bottom of pier	-2.866
	Section break	-0.891	Section break	-3.372
	Root section of box girder	-0.168	Root section of box girder	-0.553
With straining beam of wind bracing	Bottom of pier	-0.457	Bottom of pier	-1.762
	Section break	-0.327	Section break	-1.633
	Root section of box girder	-0.153	Root section of box girder	-0.284

III. B. 3) Wind resistance performance analysis

Based on the calculation results of Table 2 and Table 3 for wind analysis, three analysis results can be obtained:

(1) For the displacement and stress response of the super-high pier under wind load, the effect under dynamic wind load is more than 3.12 times larger than that under static wind load.

(2) The structural measure of wind-supported transverse girder between two box girders can significantly reduce the structural stress and displacement response under transverse wind load, with a maximum reduction of 56.42%. At the same time, it effectively improves the stress state of the super-high pier stiffness mutation cross-section, so that the wind-resistant performance of Rigid-Frame Bridge is improved.

(3) Under the condition of wind braced transverse tie beam structure, the top of the pier pier in the maximum cantilever stage, the lateral maximum displacement of 12.9cm, the bottom of the pier pier cross-section stress is 1.762MPa tensile stress, not more than the permissible value, which indicates that this paper this Rigid-Frame Bridge structural design optimization in the wind resistance of this aspect of the performance of the particularly significant.

(4) As the cantilever section of the T-structure continues to extend, the windward area increases, and the effect caused by wind load also increases gradually. In the case of the actual bridge conditions permit, for the left and right split continuous Rigid-Frame Bridge, through the addition of wind bracing transverse tie beam structure can effectively enhance the lateral wind performance of the high pier.

Overall, this paper Rigid-Frame Bridge structural design optimization process at the same time consider the wind pressure contour change and impact on the super-high pier single T structure, its response output better reflect the super-high pier has special wind dynamic characteristics, at the same time increase the wind strut beam structure can significantly reduce the top of the pier under the wind load displacement, it is worthwhile to draw reference from the same type of bridge wind design.

III. C. Construction technology simulation analysis

In this subsection, we will investigate the construction technology proposed in Section 2.3 for the wind-resistant performance of rigid-frame bridges from the perspectives of linear control and stress control of main girders, and the specific research contents are the division of construction phases, the comparative analysis of linear control (comparison between measured and theoretical values), and the comparative analysis of stress control (comparison between measured and theoretical values), and the clearer analytical process will be given in the following sections.

III. C. 1) Construction phasing

According to the actual construction requirements, the whole bridge is divided into a total of 74 construction stages, and the main work content of each stage is shown in Table 4.

Table 4: Construction phase division table

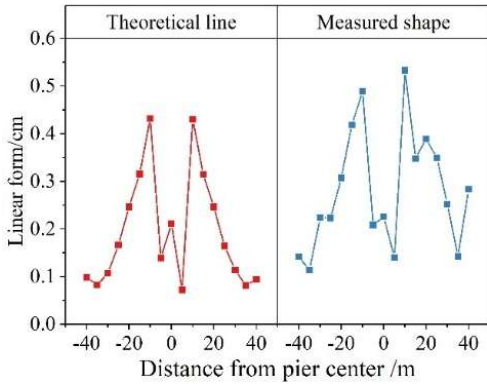
Construction phase number	Main work content
CS1	4#, 5# pier construction
CS2	0# block pouring
CS3	The 0# block prestressed bundle is tensioned
CS4	Assemble and debug the basket on the 0# block
CS5	With the T structure on pier 4# and pier 5 as the symmetry center, the beam section 1# was symmetrically poured synchronously
CS6	1# block prestressed bundle tensioned
CS7~CS63	From 2 to 9# beam sections, the following process is used to complete the cycle, in turn, the forward hanging basket, synchronous alignment Casting 2~9# beam segments and tensioning the prestressed steel bundles of the corresponding beam segments
CS64~CS67	The side span hanging basket is removed, the side span cast-in-place section is poured, and the side span closing hanger is installed
CS68~CS69	Close the side span, stretch the side span prestressed steel bundle, install the side span permanent support, remove the side span temporary support and temporary locking
CS69~CS70	Remove the middle span hanging basket, install the middle span closing hanger and apply horizontal top thrust, and close the middle span. Stretch the mid-span prestressed steel bundles and remove the closing hangers
CS71~CS72	Second stage paving
CS73~CS74	10 years of shrinkage and creep

III. C. 2) Linear control analysis of main girder

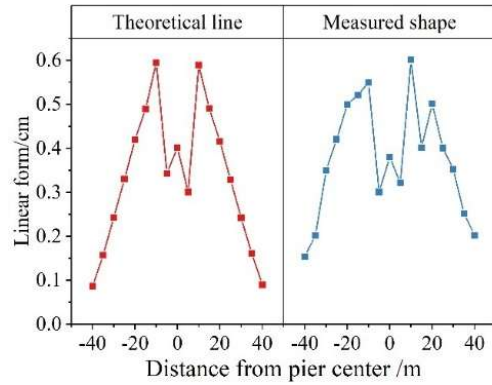
No matter what kind of construction program is applied, the girder will be displaced downward due to self-weight, shrinkage creep and other factors, which leads to the deviation between the actual position of the girder and the ideal state, and finally leads to the bridge not being able to merge smoothly or the line of the completed bridge not meeting the design requirements. Therefore, it is necessary to control the alignment of the bridge, through carefully analyzing the measured and theoretical data, to provide the correct elevation for each section of the mold, to control the error in the allowable range, to ensure the smooth construction of the bridge. The ideal line shape of each construction stage is calculated by Midas Civil, and now the ideal line shape is compared with the measured line shape and analyzed for error. Considering the limited length of the article, the linear changes of the end measurement points of each girder section in the four construction phases of 6# girder section, 7# girder section, 8# girder section and 9# girder section on pier 4# are analyzed, and the comparative analyses are shown in Fig. 4~Fig. 7, of which (a)~(b) are the comparison of the line shape of girder section after the concrete pouring and that of girder section after the tensioning of the prestressing tendons, respectively. Analyzing the line data in Fig. 4~Fig. 7, it can be seen that during the cantilever construction of Pier 4#1#~9# girder section, due to the measurement error, deformation of reinforcement at the measurement point and other factors, there is a certain deviation between the measured line and the theoretical line, but the deviation is less than 0.5cm and the overall line basically matches with the better control effect. Due to the extension of the bridge construction period, the line simulation can only be done for 9# beam section, and the rest of the beam section is still under continuous monitoring. 5# pier "T" structure 1# ~ 9# beam section cantilever construction phase line monitoring results also meet the specification requirements, due to space limitations, will not repeat.



Figure 4: Comparison of line shape of 4# pier 6# beam section during construction

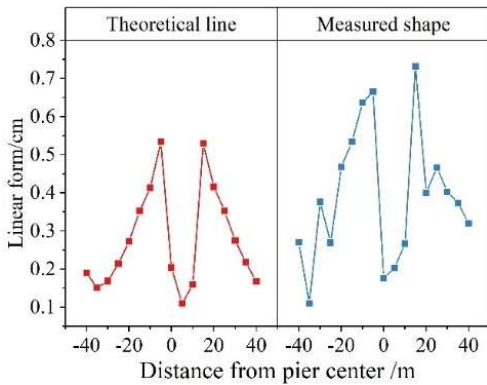


(a)Concrete placement

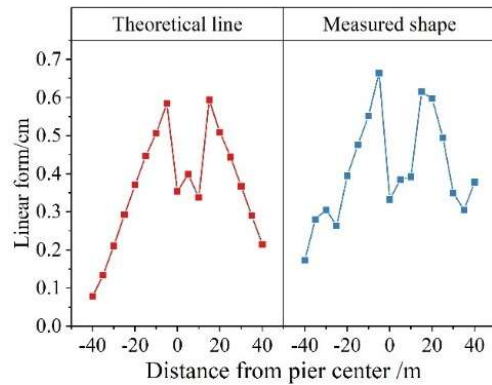


(b)Tension of prestressed tendons

Figure 5: Comparison of line shape of 4# pier 7# beam section during construction

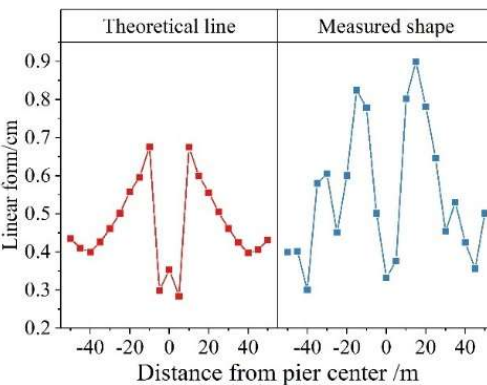


(a)Concrete placement

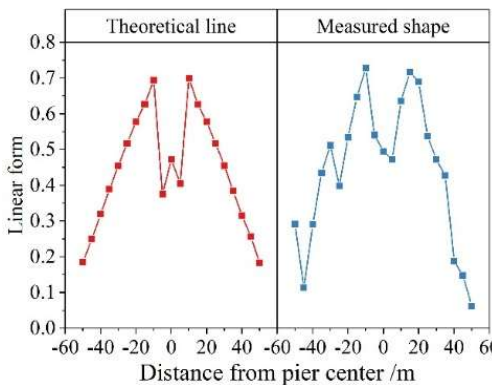


(b)Tension of prestressed tendons

Figure 6: Comparison of line shape of 4# pier 8# beam section during construction



(a)Concrete placement



(b)Tension of prestressed tendons

Figure 7: Comparison of line shape of 4# pier 9# beam section during construction

III. C. 3) Stress control analysis

Stress control is an indispensable part of bridge construction simulation analysis, which aims to ensure that the bridge is in a safe state during the construction process, and to ensure that the stress state after the bridge is

completed meets the design requirements. In the stress simulation process, the theoretical stress value and the measured stress value are compared and analyzed to determine whether the bridge stress is normal. Once the deviation between the theoretical value and the measured value is found to be large, the reason for the deviation should be found out and dealt with in time to ensure the smooth construction of the bridge.

The bridge adopts ZX-416AT buried steel stress sensor in stress monitoring, which has better stability, smaller zero drift with time, and the monitoring results can be adjusted according to the internal temperature of concrete. When the steel chord sensor is buried inside the concrete, the axial force makes the chord length between the two branch points of the steel chord change axially, which causes the self-oscillation frequency to change. The strain value of the steel string can be obtained by testing the self-oscillation frequency of the sensor and the electronic components inside the sensor, which is converted to get the stress value of the concrete at that place:

$$\sigma_c = E_e \varepsilon \quad (15)$$

where, σ_c represents the stress in the concrete structure, E_c is the modulus of elasticity of the concrete, and ε represents the strain in the steel string sensor.

$$\varepsilon = K(f_i^2 - f_0^2) \quad (16)$$

where, ε indicates the strain of the steel string sensor (10-6), K is the calibration coefficient of the sensor (10-6/Hz²), f_i is the reference value of the sensor output frequency (Hz), and f_0 is the measured value of the sensor output frequency (Hz).

The "T" structure on pier 4# of this bridge is taken as the object of study, and the measured stress value is compared with the theoretical stress value. Due to the extension of the construction period, in April 2019, only cantilever construction to 9# girder section, so selected 1# ~ 9# girder section construction process of the pier top girder section of the stress changes to be analyzed. The stress at each measurement point is positive in tension and negative in compression, and the stress monitoring results are shown in Figures 8 to 9, where (a) ~ (b) are the top plate stress and bottom plate stress, respectively. Based on the data in Fig. 8~Fig. 9, it can be seen that during the cantilever construction of 1#~9# girder segments of Pier 4#, the bottom plate is in tensile state after the tensioning of 1#~4# girder segments, but the tensile stress is small, and it will not affect the structural safety. The top plate is in compression state, which is in line with the stress characteristics of the cantilever stage of the main girder, and the change rule of the measured stress value of each girder section is generally similar to the theoretical stress value. As the cantilever construction continues, the bottom plate stress value maintains the trend of increasing all the time, and the growth rate is larger in 1#~6# beam sections, and the growth rate is relatively slow in 7#~9# beam sections. The measured stress values of the top plate and bottom plate at the cantilever stage deviate from the theoretical stress values to a certain extent, which is due to the fact that the measured stress values are affected by temperature, shrinkage and creep, but the size of the deviation is within the permissible range, which is a normal phenomenon. Due to the extension of the bridge construction period, this paper can only be implemented to the 9# beam section, the rest of the beam section is still under construction. 5# pier "T" structure 1# ~ 9# beam section cantilever construction stage of the stress monitoring results are also in line with the specifications, due to space limitations, will not be repeated. This shows that the main girder is in a safe condition with good stress state during the cantilever construction of 1#~9# girder sections.

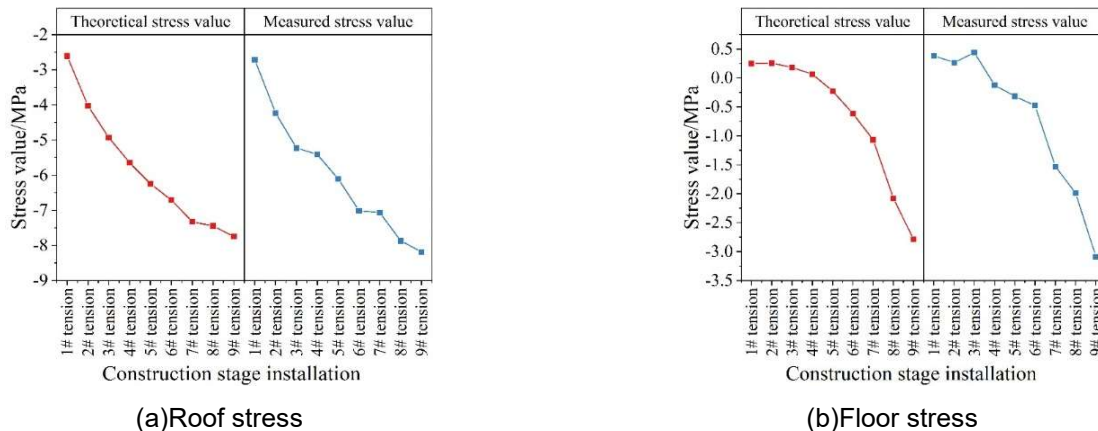


Figure 8: 4# pier small mileage pier top section stress

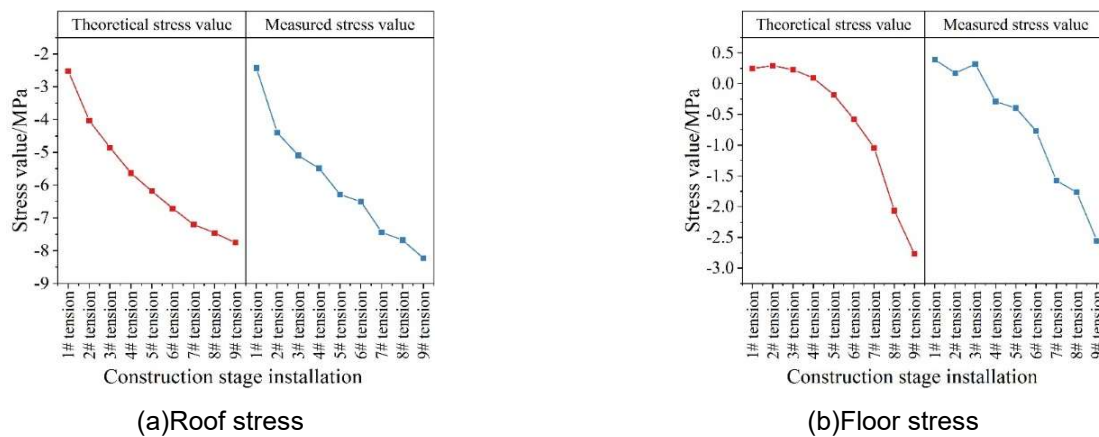


Figure 9: 4# pier large mileage pier top section stress

IV. Conclusion

In order to improve the wind resistance performance of Rigid-Frame Bridge, this paper combines the actual engineering background of a Rigid-Frame Bridge to formulate the optimization scheme of structural design and construction technology of Rigid-Frame Bridge project.

(1) The effect under dynamic wind load is more than 3.12 times larger than that under static wind load, and the maximum reduction of structural stress and displacement response under transverse wind load reaches 56.42%. In the case of the actual bridge conditions permit, increase the wind support cross-tie beam structure can effectively enhance the transverse wind performance of the high pier.

(2) The deviation of the measured and theoretical stress value (linear) of the pier top cross-section during the construction of the 1#~9# beam section is within an acceptable range, which is a good practice of the principle of safe construction, and also highlights the practicality of this paper's program in practical application.

References

- [1] Fisher, J. W., & Roy, S. (2011). Fatigue of steel bridge infrastructure. *Structure and Infrastructure Engineering*, 7(7-8), 457-475.
- [2] Liu, Y., Shen, Z., Liu, J., Chen, S., Wang, J., & Wang, X. (2022, November). Advances in the application and research of steel bridge deck pavement. In *Structures* (Vol. 45, pp. 1156-1174). Elsevier.
- [3] Zhang, Q. H., Bu, Y. Z., & Li, Q. (2017). Review on fatigue problems of orthotropic steel bridge deck. *China Journal of Highway and Transport*, 30(3), 14-30.
- [4] Wang, C., Duan, L., Zhai, M., Zhang, Y., & Wang, S. (2017). Steel bridge long-term performance research technology framework and research progress. *Advances in Structural Engineering*, 20(1), 51-68.
- [5] Wu, X., Chen, S., Hu, Y., Wang, Z., & Li, Z. (2024). Analysis and Real-Time Monitoring of the Influence of Wind Load on a High-Altitude Steel Connecting Bridge with Small Spacing. *Buildings*, 14(6), 1755.
- [6] Cheng, J., & Li, Q. S. (2009). Reliability analysis of long span steel arch bridges against wind-induced stability failure. *Journal of Wind Engineering and Industrial Aerodynamics*, 97(3-4), 132-139.
- [7] Zdravkov, L. A. (2022). Wind loads on girder bridges. *CHALLENGE*, 8(1), 9-16.
- [8] Xu, Y. L. (2013). Wind effects on cable-supported bridges. John Wiley & Sons.
- [9] Yu, E., Xu, G., Han, Y., Hu, P., Townsend, J. F., & Li, Y. (2022). Bridge vibration under complex wind field and corresponding measurements: A review. *Journal of traffic and transportation engineering (English edition)*, 9(3), 339-362.
- [10] Hua, X., Wang, C., Li, S., & Chen, Z. (2020). Experimental investigation of wind-induced vibrations of main cables for suspension bridges in construction phases. *Journal of Fluids and Structures*, 93, 102846.
- [11] Zhang, Y., Cardiff, P., & Keenahan, J. (2021). Wind-induced phenomena in long-span cable-supported bridges: a comparative review of wind tunnel tests and computational fluid dynamics modelling. *Applied Sciences*, 11(4), 1642.
- [12] Li, S., Laima, S., & Li, H. (2017). Cluster analysis of winds and wind-induced vibrations on a long-span bridge based on long-term field monitoring data. *Engineering Structures*, 138, 245-259.
- [13] Buljac, A., Kozmar, H., Pospíšil, S., & Macháček, M. (2017). Aerodynamic and aeroelastic characteristics of typical bridge decks equipped with wind barriers at the windward bridge-deck edge. *Engineering structures*, 137, 310-322.
- [14] Kim, S. J., Shim, J. H., & Kim, H. K. (2020). How wind affects vehicles crossing a double-deck suspension bridge. *Journal of Wind Engineering and Industrial Aerodynamics*, 206, 104329.
- [15] Fujino, Y., Kimura, K., Tanaka, H., Fujino, Y., Kimura, K., & Tanaka, H. (2012). Wind resistant design codes for bridges in Japan. *Wind Resistant Design of Bridges in Japan: Developments and Practices*, 1-7.
- [16] Zhou, Q., & Zhu, L. D. (2020). Numerical and experimental study on wind environment at near tower region of a bridge deck. *Heliyon*, 6(5).
- [17] Wright, W. J. (2012). *Steel bridge design handbook: Bridge steels and their mechanical properties* (No. FHWA-IF-12-052). United States. Federal Highway Administration. Office of Bridge Technology.
- [18] Gao, W. B., Su, Q. K., Zhang, J. W., Xie, H. B., Wen, F., Li, F., & Liu, J. Z. (2020). Steel Bridge Construction of Hong Kong–Zhuhai–Macao Bridge. *International Journal of Steel Structures*, 20(5), 1498-1508.



- [19] Chavel, B. W. (2012). Steel bridge design handbook: Bridge deck design (No. FHWA-IF-12-052). United States. Federal Highway Administration. Office of Bridge Technology.
- [20] Xian, J., He, J., Zhu, S., & Zhong, M. (2022, April). A Study on Wind Resistance of Steel Arch Pedestrian Bridge. In International Conference on Green Building, Civil Engineering and Smart City (pp. 1045-1052). Singapore: Springer Nature Singapore.
- [21] Gao Zhang, Jin Zhang, Yang Liu & Yating Cao. (2024). Seismic fragility analysis of long-span rigid-frame bridge on mountainous soft clay site. *Advances in Bridge Engineering*(1),25-25.
- [22] Yixiang Liu, Lingbo Wang, Cong Jiang & Hao Shu. (2024). Research on Mechanical Performance of In-Service Continuous Rigid-Frame Bridge Based on Vehicle-Bridge Coupling Vibration. *Applied Sciences*(16),6950-6950.
- [23] Xiangcheng Sun, Keichi Takahashi, Yoichi Shimomura, Hiroyuki Takizawa & Xian Wang. (2025). Performance evaluation of the LBM simulations in fluid dynamics on SX-Aurora TSUBASA vector engine. *Computer Physics Communications*109411-109411.